

# Method for Improved Fluorescence Corrections for Molar Mass Characterization by Multiangle Light Scattering

Zachariah A. Pittman,\* Madeline E. McCarthy, Marc R. Birtwistle, and Christopher L. Kitchens\*



Cite This: *Biomacromolecules* 2022, 23, 3743–3751



Read Online

ACCESS |



Metrics & More

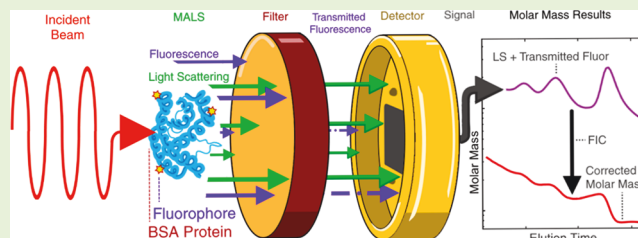


Article Recommendations



Supporting Information

**ABSTRACT:** Multiangle light scattering (MALS) was used to determine the absolute molar mass of fluorescent macromolecules. It is standard protocol to install bandwidth filters before MALS detectors to suppress detection of fluorescent emissions. Fluorescence can introduce tremendous error in light scattering measurements and is a formidable challenge in accurately characterizing fluorescent macromolecules and particles. However, we show that for some systems, bandwidth filters alone are insufficient for blocking fluorescence in molar mass determinations. For these systems, we have devised a correction procedure to calculate the amount of fluorescence interference in the filtered signal. By determining the intensity of fluorescent emission not blocked by the bandwidth filters, we can correct the filtered signal accordingly and accurately determine the true molar mass. The transmission rates are calculated before MALS experimentation using emission data from standard fluorimetry techniques, allowing for the characterization of unknown samples. To validate the correction procedure, we synthesized fluorescent dye-conjugated proteins using an IR800CW (LI-COR) fluorophore and Bovine Serum Albumin protein. We successfully eliminated fluorescence interference in MALS measurements using this approach. This correction procedure has potential application toward more accurate molar mass characterizations of macromolecules with intrinsic fluorescence, such as lignins, fluorescent proteins, fluorescence-tagged proteins, and optically active nanoparticles.



## INTRODUCTION

When light propagates through a medium, it creates an oscillating electric field that induces oscillating dipoles in molecules that it passes through. The oscillating dipoles within molecules create electromagnetic fields—thus emitting light, a phenomenon known as light scattering (LS). Our focus lies with elastic light scattering (Rayleigh scattering), where there is no change in the wavelength of the emitted light from the incident light. Most importantly, Rayleigh scattering can be used to determine the molar mass of a molecule. The relationship between molar mass and scattered light of molecules in a dilute solution when using the Rayleigh-Gan-Debye approximation<sup>1</sup> (RGD) is given.

$$R_{\theta} = K^*McP(\theta)[1 - 2A_2McP(\theta)] \quad (1a)$$

$$K^* = 4\pi^2 n_0^2 \frac{(dn/dc)^2}{\lambda^4 N_A} \quad (1b)$$

where  $R_{\theta}$  ( $\text{cm}^{-1}$ ) is the excess Rayleigh ratio as measured by a detector at angle  $\theta$ ,  $M$  is the weight-average molar mass (g/mol),  $P(\theta)$  is the form factor,  $K^*$  is the optical constant, and  $c$  is the concentration. Elaborations on RGD can be found elsewhere in the literature.<sup>1,2</sup> For large molecules ( $R_g \geq$  about 10 nm for a 658 nm laser),<sup>1</sup> the scattered light intensity will have an angular dependence, represented in  $P(\theta)$ . Theoretically, all size and shape effects vanish ( $P(\theta) \rightarrow 1$ ) when

intensities are measured at the same angle as the incident beam ( $\theta = 0^\circ$ ), however, measuring scattering at  $\theta = 0^\circ$  cannot be done in practice without also measuring the intensity of the incident light.<sup>1</sup> Instead, multiple angles about the illuminated sample can be measured and then extrapolated to  $0^\circ$  to arrive at a size and shape independent of molar mass: this is called multiangle light scattering (MALS). By examining the angular dependence and angular variation of scattered light, we can also determine the radius of gyration and shape, respectively. However, shape information is limited to very large macromolecules. A combination of MALS with an online fractionation technique such as size-exclusion chromatography (SEC-MALS), is often used to characterize disperse solutions and is employed in this study. This technique allows for the additional determination of the number-average molar mass ( $M_n$ ) and dispersity ( $\mathcal{D}$ ,  $M_w/M_n$ ).

Fluorescent macromolecules and nanoparticles are prevalent in biological, chemical, and medical fields, where fluorescent light is emitted and can significantly obscure scattered light

Received: May 11, 2022

Revised: July 22, 2022

Published: August 4, 2022





Table of Contents

Table of Contents				Table of Contents			
Table of Contents	Table of Contents	Table of Contents	Table of Contents	Table of Contents	Table of Contents	Table of Contents	Table of Contents
5	5	88	I 6	8	8-	5(	
8	@	(	8. D	?	@	8B	
@	:	??	(	9	:.	??	
?	D	: I	: (	-	9?	95	
:	B	D	D	5.	- 5	- .	
9	55	B.	B.	58	B	B	
D	5@	5. -	5. B	5?	55I	58.	
-	5:	589	5@	59	5@	5?.	
B	5D	5? 5	5? B	5-	5? I	5: I	

Table of Contents

Table of Contents

$$R_{\theta S} = N_{\theta} A_{CSCC} \left[ \frac{(V_{\theta S} - V_{\theta, baseline})}{V_{LM}} \right] \quad (2)$$

Table of Contents

$$R_{\theta, filtered} = R_{\theta S} + R_{\theta F} \quad (3)$$

$$R_{\theta, filtered} = R_{\theta S} + T_f R_{\theta F} \quad (4)$$

Table of Contents

$$R_{\theta S} = \left( \frac{R_{\theta, filtered}}{1 - T_f} \right) - \left( \frac{T_f R_{\theta, unfiltered}}{1 - T_f} \right) \quad (5)$$

Table of Contents

## 2. Table of Contents

Table of Contents

$$R_{\theta} = R_{\theta S} + R_{\theta F} \quad (6)$$

$$R_{\theta F} = N_{\theta} A_{CSCC} \left[ \frac{(V_{\theta F} - V_{\theta, baseline})}{V_{LM}} \right] \quad (7)$$



Figure 1 shows the molecular weight distribution (MWD) curves of BSA-I and BSA-II (0.03, 0.06, 0.10) at different elution times. The y-axis represents Molar Mass (g/mol)  $\times 10^5$  and the x-axis represents Elution Time (min). The curves are labeled I, II, III, and IV from left to right, indicating increasing molecular weight. BSA-I is shown as a red line, and BSA-II samples are shown as black lines with varying concentrations.

Sample	5. HBS	58HBS	5SB	5. HBS	58HBS	5SB	5. HBS	5@H	5SB	8@H
BSA-I	5. HBS	58HBS	5SB	5. HBS	58HBS	5SB	5. HBS	5@H	5SB	8@H
BSA-II 0.03	5. HBS	5@H	5SB	9D H	D 8S	5S5	5. HBS	58HBS	5SB	8@H
BSA-II 0.06	5. HBS	5@H	5SB	5S?B	58D	5S5	5. HBS	58D	5SD	8@H

Figure 1: MWD curves of BSA-I and BSA-II at different elution times.

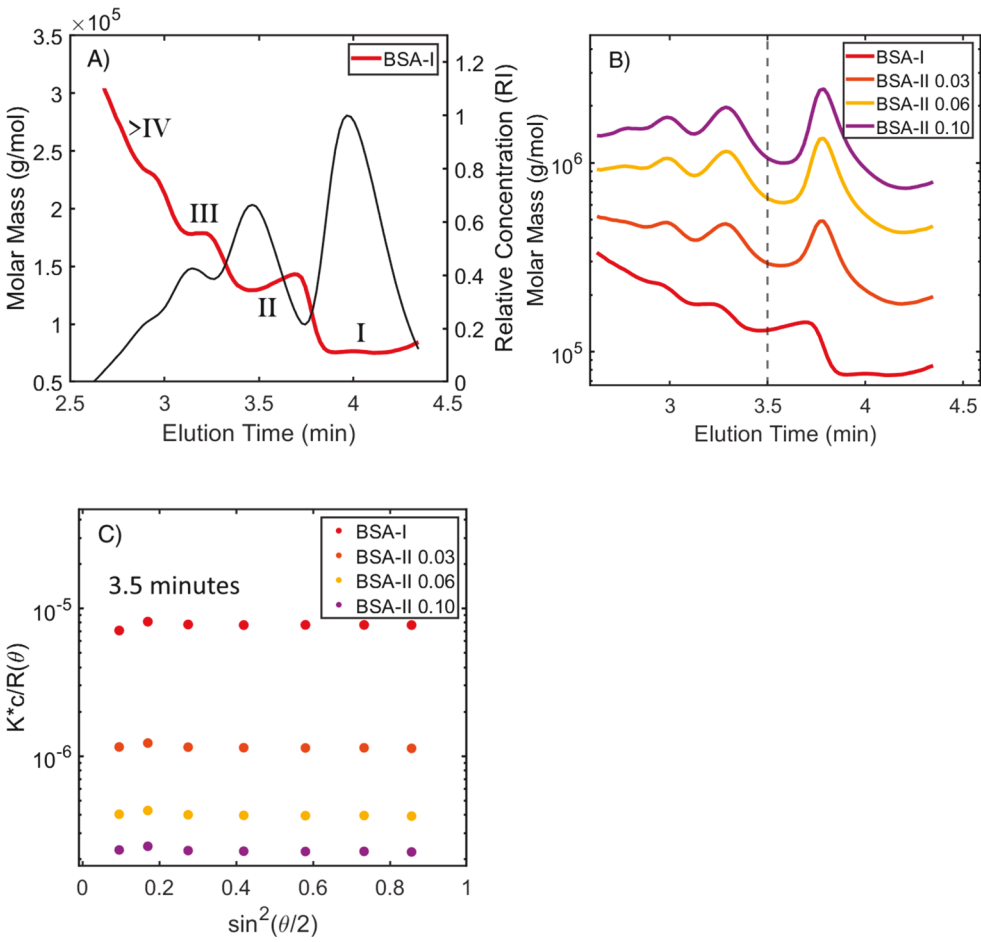


Figure 2 shows the relative mass concentration (RI) curves of BSA-I and BSA-II (0.03, 0.06, 0.10) at different elution times. The y-axis represents Relative Mass Concentration (RI) and the x-axis represents Elution Time (min). The curves are labeled BSA-I, BSA-II 0.03, BSA-II 0.06, and BSA-II 0.10. BSA-I is shown as a red line, and BSA-II samples are shown as orange, yellow, and purple lines.

### Figure 3: K\*c/R(theta) vs sin^2(theta/2) for BSA-I and BSA-II at different concentrations.

Figure 3 shows the K\*c/R(theta) curves of BSA-I and BSA-II (0.03, 0.06, 0.10) at different elution times. The y-axis represents K\*c/R(theta) and the x-axis represents sin^2(theta/2). The data points are labeled BSA-I, BSA-II 0.03, BSA-II 0.06, and BSA-II 0.10. The concentration is 3.5 minutes.

Figure 1 shows SDS-PAGE analysis of BSA-I and BSA-II at concentrations of 0.03, 0.06, and 0.10. The gel shows a single band for each sample, indicating that the protein is pure and stable under the conditions used. The molecular weight of the bands is approximately 66 kDa, which is consistent with the expected molecular weight of BSA.

Figure 2 shows SEC analysis of BSA-I and BSA-II at concentrations of 0.03, 0.06, and 0.10. The elution time for all samples is approximately 3.5 minutes, indicating that the protein is monomeric and stable under the conditions used. The molecular weight of the protein is approximately 66 kDa, which is consistent with the expected molecular weight of BSA.

Figure 3 shows UV-Vis spectra of BSA-I and BSA-II at concentrations of 0.03, 0.06, and 0.10. The absorbance at 280 nm is approximately 0.1, 0.2, and 0.3 for the 0.03, 0.06, and 0.10 concentrations, respectively. The absorbance at 280 nm is proportional to the protein concentration, and the results are consistent with the expected absorbance of BSA at this concentration.

Figure 4 shows the effect of BSA-I and BSA-II on the activity of the enzyme. The activity of the enzyme is measured by the amount of substrate converted to product over time. The results show that the activity of the enzyme is significantly higher in the presence of BSA-I and BSA-II compared to the control. This suggests that BSA-I and BSA-II act as cofactors for the enzyme.

Figure 5 shows the effect of BSA-I and BSA-II on the stability of the enzyme. The stability of the enzyme is measured by the amount of activity remaining after a certain period of time. The results show that the activity of the enzyme is significantly higher in the presence of BSA-I and BSA-II compared to the control. This suggests that BSA-I and BSA-II act as stabilizers for the enzyme.

Figure 6 shows the effect of BSA-I and BSA-II on the thermal stability of the enzyme. The thermal stability of the enzyme is measured by the amount of activity remaining after a certain period of time at a higher temperature. The results show that the activity of the enzyme is significantly higher in the presence of BSA-I and BSA-II compared to the control. This suggests that BSA-I and BSA-II act as thermal stabilizers for the enzyme.

Figure 7 shows the effect of BSA-I and BSA-II on the pH stability of the enzyme. The pH stability of the enzyme is measured by the amount of activity remaining after a certain period of time at a higher pH. The results show that the activity of the enzyme is significantly higher in the presence of BSA-I and BSA-II compared to the control. This suggests that BSA-I and BSA-II act as pH stabilizers for the enzyme.

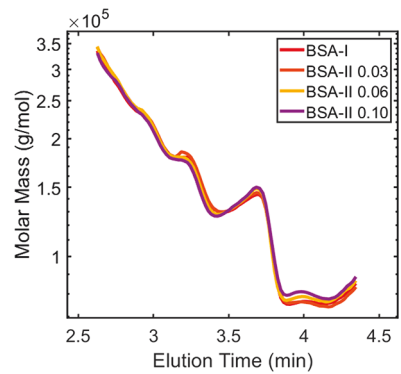


Figure 2: SEC analysis of BSA-I and BSA-II at various concentrations. The elution time for all samples is approximately 3.5 minutes, indicating that the protein is monomeric and stable under the conditions used.

Figure 3 shows UV-Vis spectra of BSA-I and BSA-II at concentrations of 0.03, 0.06, and 0.10. The absorbance at 280 nm is approximately 0.1, 0.2, and 0.3 for the 0.03, 0.06, and 0.10 concentrations, respectively. The absorbance at 280 nm is proportional to the protein concentration, and the results are consistent with the expected absorbance of BSA at this concentration.

Figure 4 shows the effect of BSA-I and BSA-II on the activity of the enzyme. The activity of the enzyme is measured by the amount of substrate converted to product over time. The results show that the activity of the enzyme is significantly higher in the presence of BSA-I and BSA-II compared to the control. This suggests that BSA-I and BSA-II act as cofactors for the enzyme.

Figure 5 shows the effect of BSA-I and BSA-II on the stability of the enzyme. The stability of the enzyme is measured by the amount of activity remaining after a certain period of time. The results show that the activity of the enzyme is significantly higher in the presence of BSA-I and BSA-II compared to the control. This suggests that BSA-I and BSA-II act as stabilizers for the enzyme.

Figure 6 shows the effect of BSA-I and BSA-II on the thermal stability of the enzyme. The thermal stability of the enzyme is measured by the amount of activity remaining after a certain period of time at a higher temperature. The results show that the activity of the enzyme is significantly higher in the presence of BSA-I and BSA-II compared to the control. This suggests that BSA-I and BSA-II act as thermal stabilizers for the enzyme.

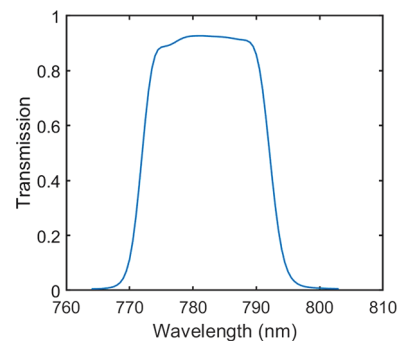
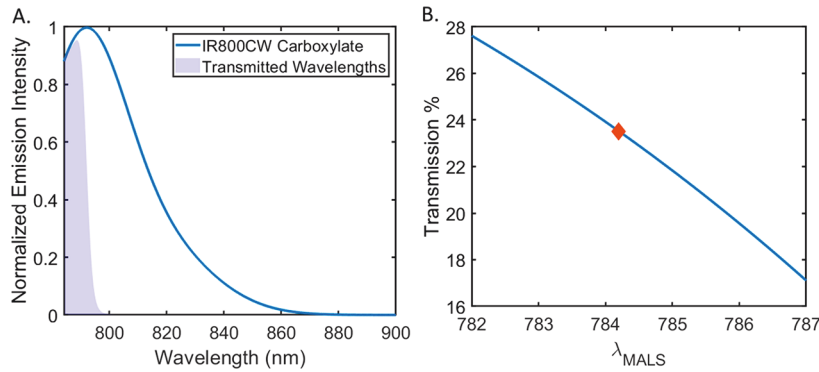


Figure 3: UV-Vis spectra of BSA-I and BSA-II at various concentrations. The absorbance at 280 nm is approximately 0.1, 0.2, and 0.3 for the 0.03, 0.06, and 0.10 concentrations, respectively.



2. 7. ... / 0 ...

IR800CW Carboxylate ... I ...

3. 4. ... 3. ... 5. (6)

...	...
...	...
...	...
...	...

$$T_f = \frac{\int_{\lambda_{MALS}}^{\infty} I_f(\lambda) \cdot T_B(\lambda)}{\int_{\lambda_{MALS}}^{\infty} I_f(\lambda)}$$

... DB: ... Q.5. ...

... ( ... ) ...

E. ... / M ...

... @ ...

0. ... / 0 ...

Text block 1: Introduction and context of the document.

Text block 2: Detailed description of the project or process.

Text block 3: Further details and technical specifications.

Section 2: Key points and objectives.

Text block 4: Summary and concluding remarks.

Text block 5: Additional information and notes.

Section 2: Key points and objectives.

Text block 6: Specific details and data points.

Text block 7: Further details and technical specifications.

Section 2: Key points and objectives.

Text block 8: Specific details and data points.

Text block 9: Further details and technical specifications.

Section 2: Key points and objectives.

Text block 10: Specific details and data points.

Text block 11: Additional information and notes.

Section 2: Key points and objectives.

Text block 12: Specific details and data points.

Section 2: Key points and objectives.

Text block 13: Additional information and notes.

Section 2: Key points and objectives.

Text block 14: Summary and concluding remarks.



able Energy (EERE) Bio-Energy Technologies Office (BETO) under Agreement No. EE0008502. Graham C. Tindall is gratefully acknowledged for his time and thoughtful discussions that greatly helped in the development and execution of this work and for providing the hybrid poplar lignin. This project is also part of activities with Mark C. Thies and is thanked for his continued support.

## REFERENCES

- (1) Wyatt, P. J. Light Scattering and the Absolute Characterization of Macromolecules. *Anal. Chim. Acta* **1993**, *272* (1), 1–40.
- (2) Berry, G. C. Total Intensity Light Scattering from Solutions of Macromolecules. *Soft Matter Charact.* **2008**, November (2004), 41–131.
- (3) Zinovyev, G.; Sulaeva, I.; Podzimek, S.; Rössner, D.; Kilpeläinen, I.; Sumerskii, I.; Rosenau, T.; Potthast, A. Getting Closer to Absolute Molar Masses of Technical Lignins. *ChemSusChem* **2018**, *11* (18), 3259–3268.
- (4) Some, D. W. T. WP9002: Fluorescent Macromolecules and Nanoparticles: Characterization of Molar Mass, Size and Charge. Wyatt Whitepaper. <https://wyattfiles.s3-us-west-2.amazonaws.com/literature/white-papers/WP9002-Characterization-of-fluorescent-macromolecules-and-nanoparticles.pdf>.
- (5) Gaugler, E. C.; Radke, W.; Vogt, A. P.; Smith, D. A. Molar Mass Determination of Lignins and Characterization of Their Polymeric Structures by Multi-Detector Gel Permeation Chromatography. *J. Anal. Sci. Technol.* **2021**, *12*, 30.
- (6) Dong, D.; Fricke, A. L. Investigation of Optical Effect of Lignin Solution and Determination of  $\bar{M}_w$  of Kraft Lignin by LALLS. *J. Appl. Polym. Sci.* **1993**, *50* (7), 1131–1140.
- (7) Ono, Y.; Nakamura, Y.; Zhou, Y.; Horikawa, Y.; Isogai, A. Linear and Branched Structures Present in High-Molar-Mass Fractions in Holocelluloses Prepared from Chara, Haircap Moss, Adiantum, Ginkgo, Japanese Cedar, and Eucalyptus. *Cellulose* **2021**, *28* (7), 3935–3949.
- (8) Gidh, A. V.; Decker, S. R.; See, C. H.; Himmel, M. E.; Williford, C. W. Characterization of Lignin Using Multi-Angle Laser Light Scattering and Atomic Force Microscopy. *Anal. Chim. Acta* **2006**, *555* (2), 250–258.
- (9) Mikame, K.; Funaoka, M. Polymer Structure of Lignophenol II - Comparison of Molecular Morphology of Lignophenol and Conventional Lignins. *Polym. J.* **2006**, *38* (6), 592–596.
- (10) Ruiz, M.; Valette, J.; Broust, F.; Bonfils, F. Rapid Quantification and Characterization of the Pyrolytic Lignin Fraction of Bio-Oils by Size Exclusion Chromatography Coupled with Multi-Angle Laser Light Scattering Detector (SEC-MALS). *J. Anal. Appl. Pyrolysis* **2019**, *142* (March), 104662.
- (11) Ralph, J.; Peng, J.; Lu, F.; Hatfield, R. D.; Helm, R. F. Are Lignins Optically Active? *J. Agric. Food Chem.* **1999**, *47* (8), 2991–2996.
- (12) Kelly, K. L.; Coronado, E.; Zhao, L. L.; Schatz, G. C. The Optical Properties of Metal Nanoparticles: The Influence of Size, Shape, and Dielectric Environment. *J. Phys. Chem. B* **2003**, *107* (3), 668–677.
- (13) Ureña-Benavides, E. E.; Kitchens, C. L. Static Light Scattering of Triaxial Nanoparticle Suspensions in the Rayleigh-Gans-Debye Regime: Application to Cellulose Nanocrystals. *RSC Adv.* **2012**, *2* (3), 1096–1105.
- (14) Khlebtsov, N. G. Anisotropic Properties of Plasmonic Nanoparticles: Depolarized Light Scattering, Dichroism, and Birefringence. *J. Nanophotonics* **2010**, *4* (1), 041587.
- (15) McCarthy, M. E.; Anglin, C. M.; Peer, H. A.; Boleman, S. A.; Klaubert, S. R.; Birtwistle, M. R. Protocol for Creating Antibodies with Complex Fluorescence Spectra. *Bioconjugate Chem.* **2021**, *32* (6), 1156–1166.
- (16) Cehelnik, E. D.; Mielenz, K. D. Polarization Effects on Fluorescence Measurements. *J. Photochem.* **1976**, *5* (3), 159.
- (17) Shinitzky, M. Effect of Fluorescence Polarization on Fluorescence Intensity and Decay Measurements. *J. Chem. Phys.* **1972**, *56* (12), 5979–5981.
- (18) Nickel, B. On the Elimination of the Polarization Bias of the Luminescence or Transient Absorption of Photoexcited Isotropic Solutions. *J. Lumin.* **1989**, *44* (1–2), 1–18.
- (19) Wyatt, P. J. In *Multiangle Light Scattering from Separated Samples (MALS with SEC or FFF) BT - Encyclopedia of Biophysics*; Roberts, G. C. K., Ed.; Springer: Berlin, Heidelberg, 2013; pp 1618–1637; DOI: 10.1007/978-3-642-16712-6\_282.
- (20) Kiefer, J. Sequential Minimax Search for a Maximum. *Proc. Am. Math. Soc.* **1953**, *4* (3), 502.

## Recommended by ACS

### Fluorescence Recovery after Photobleaching in Colloidal Science: Introduction and Application

Aref Abbasi Moud.

FEBRUARY 24, 2022  
ACS BIOMATERIALS SCIENCE & ENGINEERING

READ 

### Luminescence-Sensitive Surfaces Bearing Ratiometric Nanoparticles for Bacteria Growth Detection

Miaobo Pan, Rachel Méallet-Renault, et al.

JULY 11, 2022  
ACS APPLIED POLYMER MATERIALS

READ 

### Chloride Interference during Analysis of Dissolved Organic Carbon Using Wet Chemical Oxidation Methods

André van Zomeren, Rob N. J. Comans, et al.

APRIL 23, 2021  
ACS ES&T WATER

READ 

### Nature of Saccharide-Induced F127 Micellar Dehydration: An Insight with FDAPT (2-Formyl-5-(4'-N,N-dimethylaminophenyl)thiophene), a Multiparametric Fluorophore

Saugata Sahu, Ashok Kumar Mishra, et al.

MARCH 02, 2021  
LANGMUIR

READ 

Get More Suggestions >